The International Journal of Advanced Manufacturing Technology (2018) 99:1839–1852
https://doi.org/10.1007/s00170-018-2628-z

ORIGINAL ARTICLE

A surface and sub-surface quality evaluation of three cast iron grades after grinding under various cutting conditions

Rosemar Batista Da Silva [1] · Mariana Landim Silveira Lima [1] · Mayara Fernanda Pereira [1] · Bruno Souza Abrão [1] · Leonardo Rosa Ribeiro Da Silva [1] · Eduardo Carlos Bianchi [2] · Alisson Rocha Machado [1,3]

Received: 13 April 2018 / Accepted: 20 August 2018 / Published online: 28 August 2018
© Springer-Verlag London Ltd., part of Springer Nature 2018

Abstract
Grinding is one of the most common finishing processes used in the manufacture of metal components that require a combination of both smooth surface finish and tight tolerances. Despite the abundant knowledge concerning this process, specific literature is still scarce regarding the grinding of different cast iron grades. These materials have a wide application in the automotive industry, notably in the manufacture of gears, crankshafts, and valve control shafts. In this sense, this paper presents an experimental study of the peripheral surface grinding of three grades of cast iron grades (gray, nodular, and compacted graphite) with two SiC abrasive grinding wheels. The input variables tested were two values for depth of cut (15 and 30 μm) and two worktable speeds (5 and 10 m/min). The output variables analyzed were surface roughness, microhardness, microstructures, and SEM images of the ground surfaces. The results showed that gray cast iron provided the best performance concerning surface and sub-surface integrity among the three cast iron grades tested, whereas the nodular cast iron exhibited both worst finishing and superficial texture. No microstructural changes were observed in the samples of gray and compacted graphite cast iron grades, irrespective of the cutting conditions investigated, unlike for the nodular cast iron grade in which microstructural change was detected. The ranking order for the grindability of the three cast iron grades in terms of roughness, microhardness and surface texture investigated in this paper is gray cast iron, compacted graphite iron and nodular cast iron.

Keywords Grinding · Cast iron · Grindability · Depth of cut · Worktable speed · Surface and sub-surface qualities · SEM images

1 Introduction

In the current scenario of industrial competitiveness, there is a growing demand for interchangeable parts and components that require high surface quality and tight tolerances [1]. Many of the current research studies directed toward the improvement of cast iron mechanical properties and its manufacturing processes are being developed to support the growing demand for this material in replacing steel alloys, especially in the automotive industry [2].

✉ Rosemar Batista Da Silva
rosemar.silva@ufu.br

Mariana Landim Silveira Lima
mariana_lan7@hotmail.com

Mayara Fernanda Pereira
mayaraufu2011@gmail.com

Bruno Souza Abrão
brunoabrao53@gmail.com

Leonardo Rosa Ribeiro Da Silva
leonardo.rrs@gmail.com

Eduardo Carlos Bianchi
bianchi@feb.unesp.br

Alisson Rocha Machado
alisson.rocha@pucpr.br

[1] School of Mechanical Engineering, Federal University of Uberlandia, Av. João Naves de Ávila, 2121, Campus Santa Mônica, Uberlandia, MG 38408-100, Brazil

[2] Department of Mechanical Engineering, São Paulo State University "Júlio de Mesquita Filho", Bauru campus, Av.Eng. Luiz Edmundo C. Coube, 14-01 Vargem Limpa, Bauru, SP 17033-360, Brazil

[3] Mechanical Engineering Graduate Program, Pontifícia Universidade Católica do Paraná – PUC-PR, Curitiba, PR 80215-901, Brazil

Some particular characteristics make the cast iron group competitive when compared to steels, especially in terms of machinability and hence industrial application. Cast irons have a lower melting point, which reduces the cost of the casting process, thus providing a better heat dissipation capacity as well as absorption of vibrations; in addition, the presence of graphite provides a better lubricity, which reduces tool wear during machining [3].

Cast iron is a ternary alloy based on iron, carbon, and silicon in which iron is the principal element and carbon is contained at a minimum percentage of 2.11%. According to chemical composition and microstructure, cast irons can be classified into six groups: gray iron, nodular iron, compacted graphite iron, malleable iron, white iron, and alloyed iron, where the first three are most widely employed in industry [3]. The group of gray cast iron has a carbon content between 2.5 and 4.0 wt%, and silicon contents between 1.0 and 3.0 wt%. In their microstructure, the graphite group is in the form of flakes that are usually surrounded by a matrix of ferrite or perlite. The presence of graphite in flake form improves heat dissipation and lubricity and allows for greater stress concentration, thus reducing tenacity and consequently improving machinability [4]. Gray cast iron is the most common group of cast irons and as such they have a wide industrial application, as in the manufacturing of engine blocks, drums, and break disks [1].

Nodular cast irons are obtained by the addition of a small amount of magnesium and/or cerium to the graphitized cast iron microstructure prior to casting. These elements modify the shape of the graphite growth that appears in the form of nodes or spheroids instead of flakes. This process produces a new microstructure along with a set of different mechanical properties, which make this group competitive in regard to steels, principally in terms of ductility [4]. Due to their properties, nodular cast irons are employed in the manufacture of crankshafts, head blocks, and valves [3].

Compacted graphite iron is a modern group characterized by the presence of vermicular graphite, which is an intermediate form between flakes and nodules [3]. Vermicular graphite in these materials is rounder and coarser which constitutes a gain in terms of mechanical properties, as it highlights the mechanical and fatigue resistances with only a small loss to thermal conductivity and damping. The properties of these materials are of an intermediate level between gray and nodular cast irons [4, 5].

Furthermore, cast irons have a wide application in the automotive industry, notably in the manufacture of gears, crankshafts, and valve control shafts. These components all require high surface quality, tight tolerances, and complex sharps, which can be obtained through precision machining process, such as grinding [1]. Grinding is an abrasive machining process that generates dimensional tolerances within the ranges of International Tolerance (IT) IT6 and IT4, along with grade and roughness values varying from 0.2 to 1.6 μm [4]. In this process, thousands of abrasive grit pieces are held together by a binding material, which acts as a microcutting tool with very sharp edges. These pieces are thus forced into the workpiece material as the grinding wheel moves against the workpiece and cuts away small chips when compared to those generated by conventional machining process with tools of more defined cutting edges, such as milling [6].

The major conventional grades of abrasive materials employed in the grinding of metals are aluminum oxide (Al_2O_3) and silicon carbide (SiC). Although the former is harder and more friable than aluminum oxide, in several grinding applications, selection of an abrasive type will depend on its attritious wear resistance for a given workpiece material, rather than its hardness. The former is recommended for the grinding of high-tensile strength materials, such as alloy steel, high-speed steel, copper alloys, and ductile iron grade, while the former is suitable for grinding low-tensile strength and nonferrous metals, as well as most ceramics [6–8]. The inferior performance of silicon carbide for most ferrous applications is generally attributed to its high chemical reactivity with iron and steel alloys, which leads to poor attrition resistance and low grinding ratios. However, silicon carbide performs better than aluminum oxide on hard cast irons, where the high carbon content in the metal minimizes chemical interaction with the wheel and also due to the presence of small amounts of SiC, which is a normal constituent of iron [6].

Despite there being little information on the subject of cast iron grinding parameters, many researchers are currently developing this field. The influence of depth of cut, worktable speed, and the quantity of spheroidal graphite were evaluated on the surface roughness, residual stresses, and distortion of ductile cast iron material after the grinding operation [9]. The authors observed that the spheroidal graphite form shifts with the increase of depth of cut, which they attributed to the increase in plastic deformation, as well as to the increase in temperature along the cutting zone. They also observed that surface roughness decreased slightly with the increase in the number of spheroidal graphite nodules.

The study of residual stresses in ground materials is of great importance, as high-tensile residual stresses, for instance, are thermally driven and responsible for the occurrence of cracks on machined surfaces during grinding or when in-service loading. These stresses can compromise the component structure and lead to economic losses. In this sense, Xiao et al. [10] carried out analytic and experimental tests to determine and measure, respectively, the residual stress during the grinding of camshafts made from nodular cast iron, RC 60 grade, at various cutting conditions. For the experimental tests, two superabrasive types of CBN were employed (plated and vitrified—as it has lower grit size), wheels at a cutting speed of 100 m/s using straight oil. They varied the grinding cycles for

representing different workpiece rotation speeds (45 to 125 rpm), feed, and metal removal rates. The authors reported that for all the machining conditions tested, the behavior of residual stress on the nodular cast iron material was identical: predominance of compressive stress on the surface that rapidly changed to a tensile stress below the machined surface and then slowly decreased to a negligible tensile stress for depths in excess of 100 μm, both for simulated and measured results. They also observed that the highest tensile stresses were generated when grinding with the lowest wheel grit size, as a consequence of higher rubbing friction, even when using lower metal removal rate compared to plated CBN wheel (in which a high metal removal rate was used).

In a recent study carried out by Fernandes et al. [11], the authors investigated the grindability of ductile iron GGG-70 (270 HB of hardness) with two superabrasive grinding wheels (vitrified bond CBN type) with different friability during plunging and grinding. The main parameters tested were as follows: cutting speed (v_s) of 32 m/s, worktable speed of 23.4 m/min, and a cutting depth of 100 μm and semi-synthetic soluble oil delivered by the flood technique. They reported that the less friable grinding wheel outperformed the other in terms of surface roughness (that varied between 0.27 and 0.36 μm) and grinding wheel wear, which was attributed to micro-fracture behavior of grains during the cutting process, thus leading to lower differences in abrasive grain protruding from the cutting wheel surface along its length, thereby performing a more homogeneous cutting. When comparing hardened steel, for instance SAE52100 grade, with most cast iron grades, the presence of graphite inclusions, as well as their ferritic and pearlitic microstructures in the latter, make them more conducive to grinding, thereby improving their grindability [7].

Therefore, in this paper, an experimental study for evaluating the quality of the surface and sub-surface of three cast iron grades (gray, nodular, and compacted graphite) was carried out with two SiC abrasive grinding wheels and different input variables.

2 Experimental procedures

Grinding tests were carried out in a peripheral surface grinding machine, from the manufacturer MELLO, model P36, with a z-axis resolution of 5 μm. Three different grades of cast iron were tested as workpiece material, each possessing different Vickers hardness (HV): gray (321 ± 19 HV), nodular (179 ± 14 HV), and compacted graphite (323 ± 10 HV). They were measured prior to grinding tests. They were properly prepared in the form of rectangular bars with dimensions: 49 mm (length) × 18 mm (height) × 19 mm (width). All the cast iron grades employed in this research study were produced by the continuous casting process, in which the molten iron is placed into a feeding furnace with a water-cooled graphite die mounted to the lower face of the furnace. The bar is pulled horizontally from the furnace as the ferrostatic pressure continuously feeds molten iron through the die and the uniform microstructure of materials is enhanced by the gradual cooling process of metal in the die provided by the water. As the bar is continuously drawn from the mold through the length of the machine, the solidification process is then complete [12, 13]. One major difference among the cast iron grades tested is the presence of magnesium. In both nodular cast iron (NCI) and compacted graphite iron (CGI) grades, magnesium is responsible for the special properties of these materials. In the case of CGI grade, the complete final adjustment of magnesium and inoculant, prior to casting, is a specific characteristic of its production, since the higher magnesium content than found in the NCI grade prevents growth of graphite flakes. In the NCI grade, magnesium causes the graphite to form in a spheroid shape as opposed to the flakes of gray cast iron (GCI) grade. Although these materials are suitable for different types of heat and other surface treatments in accordance with industrial demand, for instance to improve wear and corrosion resistances, none of these materials employed in this current work were subjected to heat surface treatments [14]. In Table 1 are presented some physical and mechanical properties of the cast iron grades studied in this work.

The grinding wheels were made from a silicon carbide (SiC) material with designation 39C46KVK and 39C100KVK, which possessed the following dimensions: 254 mm (external diameter) × 25 mm (width) × 76 mm (internal diameter). Noteworthy here is that silicon carbide abrasives are recommended for the grinding of non-ferrous metals and cast irons as hard, due to the fact that brittle materials generally require a wheel with a fine grit size and a softer grade.

The input parameters used in the grinding tests were a cutting speed of 32 m/s, two values of worktable speed (v_w = 5 and 10 m/min) and depth of cut (a_e = 15 and 30 μm), which are typically those parameters employed in the grinding of steels with similar hardness as found in the cast irons tested in this study. The tests were carried out with a semi-synthetic vegetable oil-based (VASCO 7000) water-soluble cutting fluid, from Blaser Swisslube, at a dilution ratio of 1:19, in which the nozzle was positioned tangentially to the grinding wheel at a flow rate of 540 L/h. Prior to each grinding test, a dressing operation was performed through a single-point diamond dresser, being attached to the machine table by a holder in order to cover the entire thickness of the grinding wheel at a constant grinding depth of 10 μm (Table 2).

The output parameters evaluated were surface roughness, microhardness, and SEM images. The surface roughness, Ra and Rz, parameters were measured with the aid of a Mitutoyo portable perfilometer, SJ201P model, with 0.01 μm of resolution, filter wavelength (cutoff) of 0.8 mm, and evaluation length of 4.0 mm. Four roughness measurements were performed on each ground surface perpendicularly to the cutting

Table 1 Some physical and mechanical properties of gray, compacted graphite, and nodular cast iron (adapted from [15])

Properties	Tensile strength (MPa)	Young modulus (GPa)	Elongation (%)	Thermal conductivity (Wm^{-1} k^{-1})	Relative damping capacity	Hardness (BHN 10/3000)
Gray cast iron (GCI)	250	105	0	48	1	200
Nodular cast iron (NCI)	750	160	5	28	0.22	270
Compacted graphite iron (CGI)	450	145	1.5	37	0.35	255

direction and equidistant at 10 mm (Fig. 1) and the measurement average was calculated. After the grinding tests, all the samples were submitted to metallographic tests to assess their surface integrity.

Prior to the metallographic tests, the samples were subjected to a sanding process using silicon carbide sand papers with a granulometry mesh ranging from 80 to 1200. Following this, the samples were polished in an automatic rotatory machine with an alumina paste with sizes of 0.3 and 0.1 μm. Finally, the samples were cleaned with acetone PA in an ultrasonic bath cleaner to remove the remaining abrasive grit from the previous steps. With the purpose of examining the occurrence of possible alteration in the microstructure of the cast irons after grinding, a surface perpendicular to the ground surface was properly prepared through the sanding and polishing processes, thus finally subjected to etching in Nital 2% for 5 s in order to reveal the microstructure. The analyses of the surfaces and sub-surfaces of the cast irons were performed with the aid of the scanning electron microscope (SEM) model TM 3000 from Hitachi (250, 500, and 1000). Also, in order to detect grinding burns on the machined samples, they were analyzed on an optical microscope Olympus, model BX-51, with attached camera and magnification of × 45.

The microhardness of the machined samples was evaluated using the SHIMADZU HMV-2 Series microdurometer. The load applied in each test was 255.2 mN (HV 0.025) for a period of 15 s. Eight measurements were taken on three different regions after each grinding cycle for all samples. In order to obtain the values of microhardness at different depths, the measurements were initiated at 30 μm of the ground surface, with a horizontal distance between the indentations of 30 μm, as well a 20-μm indentation spacing, as shown in Fig. 2.

Table 2 Grinding and dressing conditions

Input parameters and dressing conditions	
Grinding wheels	39C46KVK and 39C100KVK
Cutting speed (v_s)	32 m/s
Worktable speed (v_w)	5 and 10 m/min
Radial depth of cut (a_e)	15 and 30 μm
Flow rate (v_j)	545 L/h
Grinding depth (a_p)	72 μm
Dressing overlap ratio (U_d)	3
Dressing depth of cut (a_d)	10 μm

3 Results and discussion

In this section, the results are presented for surface roughness, microhardness profiles, and the images of the ground surfaces obtained after the grinding of the three grades of cast iron (gray, nodular, and compacted graphite) with silicon carbide grinding wheel at various cutting conditions.

3.1 Surface roughness

The roughness results for the Ra parameter for all materials are presented in Fig. 3. They are grouped according to the radial depth of cut (a_e), worktable speed (v_w), and mesh of the SiC grinding wheel. In order to provide a greater contribution to the interpretation of the results, Table 3 presents the equivalence of the values of a_e and v_w with the equivalent chip thickness (h_{eq}).

From Fig. 3, one notes that the Ra values increased with the radial depth of cut, irrespective of the material, worktable speed, or grinding wheel tested, as excepted and generally reported in the literature. According to Malkin and Guo [6],

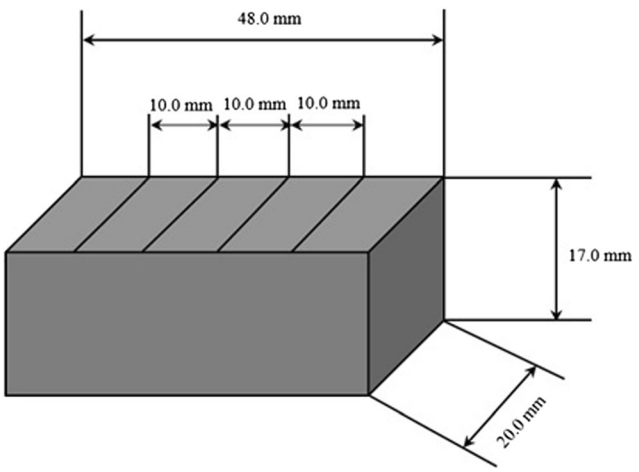

Fig. 1 Regions of the workpiece for measurements of surface roughness

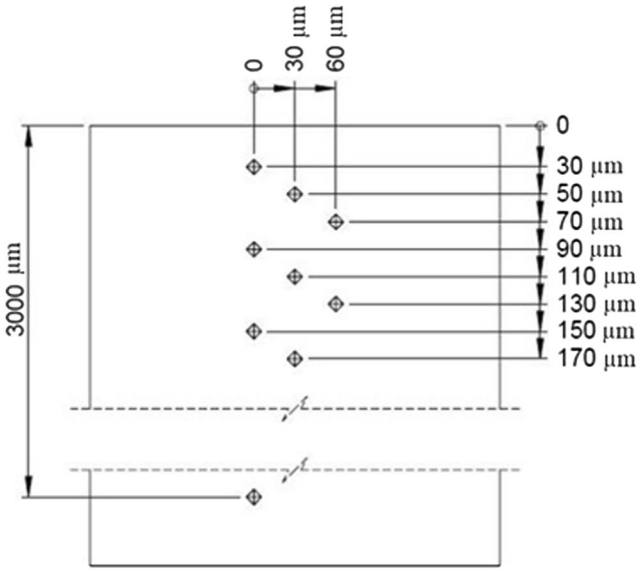

Fig. 2 Distribution of microhardness measurements

this phenomenon occurs, as initially, with a lower penetration of the grinding wheel in the workpiece, and a reduced number of grit pieces act upon the removal of material with a shorter contact time. As radial depth of cut increases, the material removal rate and the contact area increase in the same proportion as the number of grit pieces in the contact region. This leads to an increase in the cutting effort of the tool on the workpiece, raising the cutting temperature and adversely affecting the quality of the ground surface. This behavior was maintained after machining with the lowest worktable speed ($v_w = 5$ m/min) due to the lower equivalent chip thickness and longer contact time between the grinding wheel and the workpiece surface. Similarly to the effect of the radial depth of cut, the increase in the worktable speed leads to an increase in the equivalent chip thickness (h_{eq}). According to Rowe [16], the increase of this parameter causes an increase in tension on the abrasive grits. In this way, the cutting forces and the roughness of the workpiece are elevated.

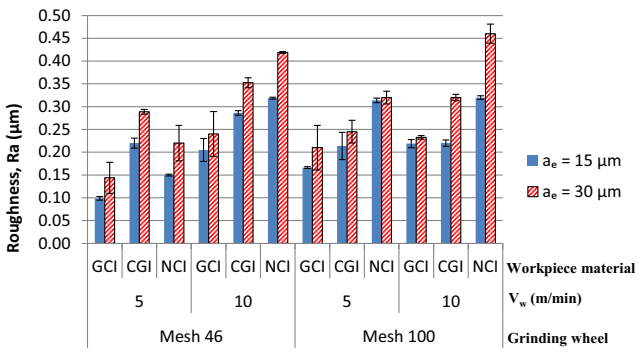

Fig. 3 Roughness values, Ra, for the three cast iron grades studied (GCI, CGI, and NCI) obtained after tangential grinding with the SiC grinding wheel and under different conditions, where GCI stands for gray cast iron, NCI for nodular cast iron, and CGI for compacted graphite iron

Table 3 Equivalence of the values of a_e and v_w with h_{eq}

v_w (m/min)	a_e (µm)	h_{eq} (µm)
5	15	0.039
	30	0.078
10	15	0.078
	30	0.156

In relation to the influence of the grinding wheel mesh, as the mesh increases, which equates to a reduction in the abrasive grit size, the values of roughness for both gray and nodular cast iron grades increase, unlike that observed for the compacted graphite iron. These results are not expected, as the smaller the grit size, the smaller the spacing between them and the smaller the amount of chip removed, which improves the surface finish [7]. However, grinding wheels with very fine grit sizes are suitable for finishing operations in which very small radial depths of cut values (< 15 µm) are used. As the radial depth of cut values used in this work varied in range of 15 and 30 µm, both the equivalent chip thickness and the chip thickness are larger than those recommended when machining with finer abrasive grits. Thus, the grinding wheel will be subject to greater shearing forces, resulting therefore in higher roughness values. In some cases, when the grinding wheel and/or the cutting conditions are not properly adjusted, the process becomes severer, and hence, more heat is generated in the cutting zone. If the cutting fluid being delivered is not efficient in the removal of heat from the grinding area, heat will be transferred, to a greater extent, to the workpiece, thus raising the temperature to the point that microstructural alteration of the workpiece material can happen, as well as other thermal damages, such as grinding burns, microcracks, tensile residual stress, and finishing deterioration. This will lead to the discarding of the workpiece material, which will consequently represent economic losses [17]. The collaborators Xiao et al. [10] carried out experimental and analytic tests in the grinding of nodular cast iron with two different sizes of CBN grit and reported an inferior performance of finer grit in terms of surface integrity, which they attributed to higher rubbing friction promoted by the higher quantity of grit in contact with the workpiece, leading to greater heat buildup on the grinding zone, which adversely affects the texture of the machined surface. Another possible explanation lies in the fact that attritious wear resistance of an abrasive grit for a given workpiece material is strongly related to its friability, i.e., the degree of grit fracture during the cutting process. According to Malkin and Guo [6], finer grits of the same material, as is the case of this study, are less friable since they are usually produced by crushing of coarser material. So, the more fragile the grits, the more susceptible they are to fracture before they are finally dislodged from the bond. If grits have low capacity to self-sharpening, they become extremely blunt, thereby

increasing grinding forces and making the workpiece more susceptible to thermal damage. In general, the ranges of the roughness values Ra obtained in this work, considering the standard deviation, were approximately 0.11 to 0.48 μm, values well below 1.00 μm, which is within the range attained for grinding processes.

Noted also is that in Fig. 3, the roughness values obtained for the compacted graphite were higher than those recorded for the gray cast iron under the conditions employed. The ductile or brittle behavior plays an important role in the formation of the chip in grinding, as well as finishing and other parameters of surface integrity and subsurface machined workpieces. Thus, the difference in roughness values for these two grades can be attributed to the higher mechanical strength of compacted graphite iron, which is almost twice as that of gray cast iron. In addition, gray cast lamellar graphite promotes the onset of fracture and its propagation, causing gray cast iron to assume a fragile behavior, whereas compacted graphite does not favor cleavage or crack propagation [5, 18]. The improved machinability of gray cast iron compared to other grades, when subjected to conventional machining processes with defined geometry tools (turning and milling, for example), has also been reported in the literature.

Another factor to be considered in relation to the chemical composition of these two materials (GCI and CGI grades) is the formation of manganese sulfide in the gray cast iron grade (GCI), which is not present in the compacted graphite iron (CGI). In gray cast iron, the sulfur reacts with the manganese (Mn) and forms inclusions of manganese sulfide (MnS) [1, 15]. In machining operations with defined geometry tools, these inclusions, during machining, are deposited on the surface of the tool and thus form a protective layer. This layer or film will act as a local solid lubricant, which consequently will favor the reduction of the friction coefficient at the chip/tool interface, serving as a barrier against tool wear [19, 20]. However, the cutting speeds during the grinding processes are much higher and the grit used in this process has smaller edges than that employed in conventional machining processes using a defined geometry tool, such as milling, and that grit used in conventional abrasives has areas of reduced contact, which hamper the permanence of the MnS inclusions on the surfaces of the abrasive grit [7]. Even with this being the case, it is believed that these inclusions may have become lodged among the grit, filling the void of the pores and also acting as lubricants in the workpiece grinding interface. As a consequence, they will stimulate a reduction in friction and improve the tribological conditions, which in turn result in a superior finish. In the case of compacted graphite iron, due to the absence of MnS, there was no formation of a lubricant layer due to the low residual value of sulfur present in the material, as well as to the fact that it combines preferentially with magnesium—nodulizing element—without a sufficient quantity remaining to combine with the manganese and form the protective layer of MnS [15]. As a result, the surface roughness value of the workpieces on this material was slightly lower.

In nodular cast iron, the presence of graphite nodules (instead of veins) gives this material relative ductility and other mechanical properties that approximate those of common carbon steels. As shown in Fig. 3, the highest surface roughness values were recorded when machining the nodular cast iron grade, which can be attributed to its relative ductility. During the grinding of materials with ductile behavior, such as common carbon steels in the annealed state or other non-metallic materials, there is a tendency for the formation of long chips. Chips can fill the voids in the grinding wheel and reduce the cutting capacity of the abrasive grit, as well as obstructing the passage of the cutting fluid on the grinding wheel surface. As a result, both the abrasive grits and the workpiece material adhered to the outermost layers of the grinding wheel will rub against the workpiece, which will deteriorate the finish. In addition, in grinding ductile materials, due to the larger area of the plastic regime, the workpiece material is also pushed to the sides of the abrasive grit, a phenomenon known as lateral material flow, and can remain on the surface of the workpiece even after machining.

According to Marwanga et al. [21], during the process of forming nodular cast iron chips, plastic deformation of the matrix among the nodules as well as the compression forces causes the nodules to detach from the matrix. The plastic deformation causes the nodules to elongate in the cutting direction, causing a ductile fracture. Thus, there is a greater tendency for the metal particles to be compressed and to adhere to the pores of the grinding wheel, thus leading to wheel clogging phenomenon. As the machining progresses, the chips on the grinding wheel surface will rub against the surface of the workpiece causing only elastic and plastic deformation of the material, leading to a reduction in the surface quality of the material. It is believed that this phenomenon occurred during the process of grinding nodular cast iron under the conditions investigated in this paper.

In order to guarantee greater statistical reliability in the roughness Ra results obtained in this research paper, an analysis of variance (ANOVA) was performed, comparing the grades of the cast iron two to two. A 95% confidence level and significance level (p value) were set at 5% for all analyses. These results are presented on Tables 4, 5, and 6.

In Table 4, one notes there is a significant difference between the results obtained for GCI and CGI and that the worktable speed, radial depth of cut, and the interactions between the material with the grinding wheel mesh and the worktable speed with the grinding wheel mesh had a significant influence on the results. In the case of CGI, the roughness increased by an average of 0.08 μm, as observed in the effect column. By increasing the worktable speed from 5 to 10 m/min, the roughness increased by an average of 0.06 μm, while

Table 4 Analysis of variance of the planning 2^4 for Ra roughness comparing the GCI and CGI

	Effect (μm)	*p* value
Material	0.077500	0.000241
v_w	0.060000	0.000803
a_e	0.051562	0.001604
Grinding wheel mesh	− 0.001875	0.830803
Material × v_w	− 0.009375	0.311458
Material × a_e	0.017188	0.094010
Material × grinding wheel mesh	− 0.036875	0.006846
v_w × a_e	0.002188	0.803313
v_w × grinding wheel mesh	− 0.023750	0.035764
a_e × grinding wheel mesh	− 0.001562	0.858570

Table 6 Analysis of variance of the planning 2^4 for Ra roughness comparing the cast iron GCI and NCI

	Effect (μm)	*p* value
Material	0.125312	0.000452
v_w	0.098750	0.002358
a_e	0.057812	0.013155
Grinding wheel mesh	0.055625	0.015253
Material × v_w	0.029375	0.114300
Material × a_e	0.023438	0.187918
Material × grinding wheel mesh	0.020625	0.237469
v_w × a_e	0.015000	0.374061
v_w × grinding wheel mesh	− 0.044406	0.035164
a_e × grinding wheel mesh	− 0.006250	0.701185

increasing the radial depth of cut from 15 to 30 μm produced an average increase of 0.05 μm.

In relation to Table 5, there is noted a significant difference between the Ra roughness results obtained for the CGI and the nodular cast iron (NCI), and that both the input variables (worktable speed and radial depth of cut) as with the interactions of the material with the worktable speed and the material with grinding wheel mesh influenced the responses significantly. Through the increase of worktable speed and radial depth of cut, the Ra roughness values also increased by an average of 0.09 and 0.08 μm, respectively. Regarding the interactions, the interaction of the material with worktable speed caused an average increase of 0.04 μm in Ra, while the interaction between the material and grinding wheel mesh produced an average increase of 0.06 μm in roughness.

In Table 6, the results for the analysis of variance between the Ra roughness values obtained for GCI and NCI are shown. One notes that the parameters of worktable speed and radial depth of cut also exerted significant influence, as observed for the other analyses (Tables 4 and 5). However, for this analysis (Table 6), the grinding wheel mesh and the interaction between it and the worktable speed also significantly influenced the response, so that when passing from the material level GCI to the NCI, the roughness values Ra increased by about 0.12 μm. By increasing the worktable speed, the average Ra response was around 0.10 μm, while the increase in radial depth of cut and grinding wheel mesh resulted in a Ra elevation of 0.06 μm. With respect to the interaction of the worktable speed with the grinding wheel mesh, the roughness value (Ra) fell by an average of 0.04 μm.

Table 5 Analysis of variance of the planning 2^4 for Ra roughness comparing the cast iron CGI and NCI

	Effect (μm)	*p* value
Material	0.047812	0.023281
v_w	0.089375	0.001802
a_e	0.075000	0.003893
Grinding wheel mesh	0.018750	0.261448
Material × v_w	0.038750	0.047538
Material × a_e	− 0.006250	0.690662
Material × grinding wheel mesh	0.057500	0.011631
v_w × a_e	0.027187	0.125952
v_w × grinding wheel mesh	− 0.035937	0.059704
a_e × grinding wheel mesh	− 0.002188	0.888392

3.2 Microhardness

In Fig. 4, fthe microhardness values are shown for the three cast iron grades gray (Fig. 4a, b), compacted graphite (Fig. 4c, d), and nodular (Fig. 4e, f), grinding with two radial depth of cut, 15 and 30 μm, and two worktable speeds, 5 and 10 m/min. The dotted line indicates the reference value of the hardness of the sample for each material prior to the grinding process (the average value for each cast iron grade was previously given in Section 2, "Experimental procedure"), while the other lines represent the average of the three values obtained for each depth below the ground surface.

The microhardness results obtained after the grinding of the gray cast iron under the various cutting conditions and with the grinding wheels mesh 46 and 100 are shown in Fig. 4a, b, respectively. Noted from Fig. 4a is that, in general, the microhardness results were kept around the average value of the material prior to grinding. In addition, a slight drop in surface microhardness of the ground material, about 8.6%, is observed after grinding under the severest machining conditions (a_e = 30 μm and v_w = 10 m/min) to the value close to 170 μm below the machined surface. However, no conclusion can be drawn for this observation, as it is known from the literature that the microstructure of gray cast iron is generally inhomogeneous due to factors related to the casting process, among others [1]. This non-homogeneity implies in areas that have a lower hardness than that of the matrix. Thus, it is believed that the sample

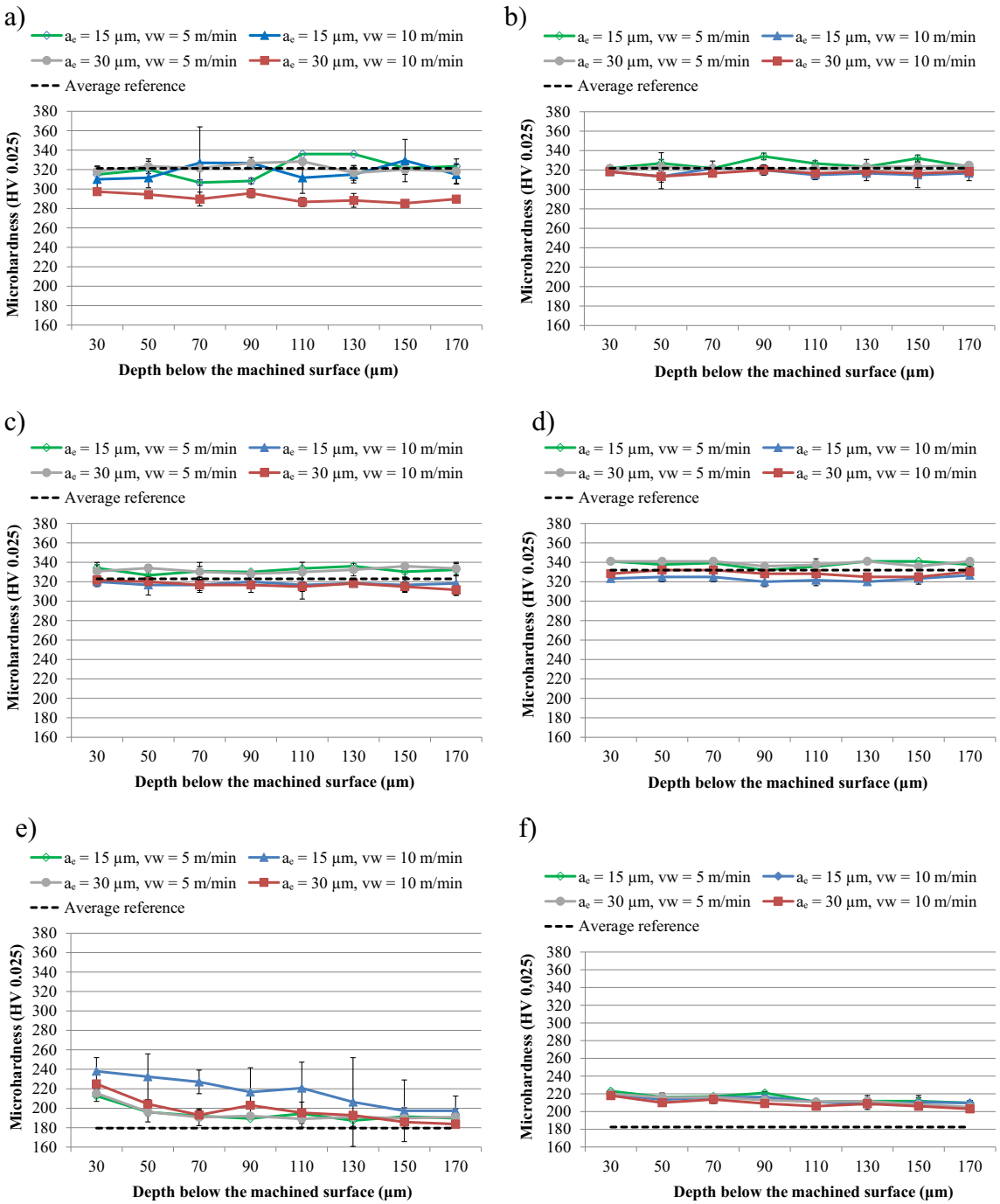

Fig. 4 Microhardness values below the surface of the three grades of cast iron. **a** Gray cast iron after grinding with mesh 46. **b** Gray cast iron after grinding with mesh 100. **c** Compacted graphite iron after grinding with mesh 46. **d** Compacted graphite iron after grinding with mesh 100. **e** Nodular cast iron after grinding with mesh 46. **f** Nodular cast iron after grinding with mesh 100

selected for this experiment is part of the region of the gray cast iron bar with the characteristics of non-homogeneity, so it is not possible to affirm that there was a decrease in the hardness of the material as a function of the grinding process under the conditions employed in this study. This fact agrees with studies on grinding carried out by Fathallah et al. [22], which also showed a slight decrease in microhardness as a consequence of the a_e increase. According to Malkin and Guo [6], the decrease in hardness can be associated with the various heating cycles followed by fast cooling that occur on the surface of the workpiece during the grinding operation that leads to formation of structures with a lower hardness than the initial one. These authors also state that if burning still does not occur, there is probability of softening taking place due to tempering occurring near the ground surface [6]. The microhardness results for the gray cast iron after grinding with the

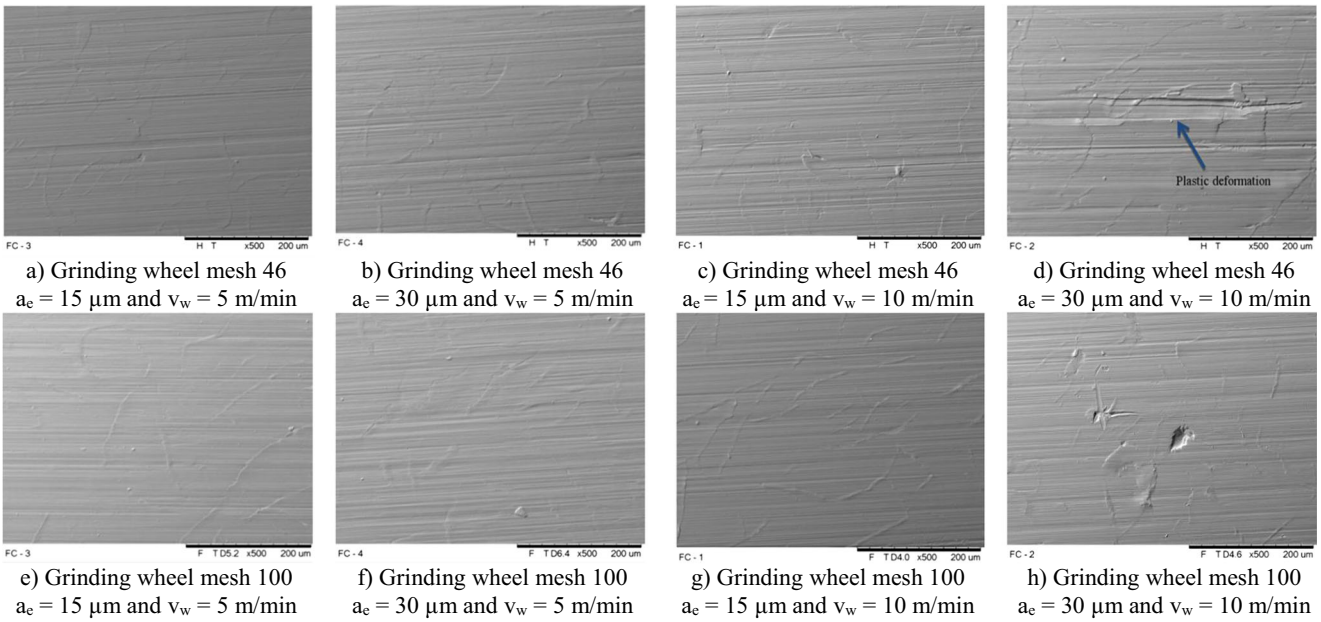

a) Grinding wheel mesh 46 a_e = 15 µm and v_w = 5 m/min
b) Grinding wheel mesh 46 a_e = 30 µm and v_w = 5 m/min
c) Grinding wheel mesh 46 a_e = 15 µm and v_w = 10 m/min
d) Grinding wheel mesh 46 a_e = 30 µm and v_w = 10 m/min
e) Grinding wheel mesh 100 a_e = 15 µm and v_w = 5 m/min
f) Grinding wheel mesh 100 a_e = 30 µm and v_w = 5 m/min
g) Grinding wheel mesh 100 a_e = 15 µm and v_w = 10 m/min
h) Grinding wheel mesh 100 a_e = 30 µm and v_w = 10 m/min

Fig. 5 Images of the surfaces of gray cast iron (GCI) ground under different cutting conditions. **a** Grinding wheel mesh 46; $a_e = 15$ µm and $v_w = 5$ m/min. **b** Grinding wheel mesh 46; $a_e = 30$ µm and $v_w = 5$ m/min. **c** Grinding wheel mesh 46; $a_e = 15$ µm and $v_w = 10$ m/min. **d** Grinding wheel mesh 46; $a_e = 30$ µm and $v_w = 10$ m/min. **e** Grinding wheel mesh 100; $a_e = 15$ µm and $v_w = 5$ m/min. **f** Grinding wheel mesh 100; $a_e = 30$ µm and $v_w = 5$ m/min. **g** Grinding wheel mesh 100; $a_e = 15$ µm and $v_w = 10$ m/min. **h** Grinding wheel mesh 100; $a_e = 30$ µm and $v_w = 10$ m/min

grinding wheel mesh 100 are shown in Fig. 4b. Although the microhardness values obtained for the severer machining conditions (higher v_w) suggest that there was a decrease in this parameter, it is not possible to affirm that there was a significant difference between the values of microhardness under the investigated conditions for gray iron.

In relation to the compacted graphite iron, the microhardness results obtained after the grinding under the different cutting conditions and with the grinding wheels mesh 46 and 100, respectively, are shown in Fig. 4c, d. One notes from Fig. 4c that there was a decrease of about 1.7% in the microhardness when grinding compacted graphite iron in relation to the reference value. For the grinding wheel mesh 100 (Fig. 4d) and at a higher worktable speed ($v_w = 10$ m/min), the percentage of decrease was near 1.8%. In general, the use of a higher worktable speed ($v_w = 10$ m/min) generated lower microhardness values than the reference value, with an average reduction of 1.8%.

The microhardness results obtained after grinding of the nodular cast iron with grinding wheels mesh 46 and 100, respectively, and under various cutting conditions are shown in Fig. 4e, f, and in the microhardness values measured below the nodular cast iron surface for all investigated conditions showed behavior different from that observed for gray cast iron and compacted graphite iron. The highest values were recorded in regions closer to the surface and they decreased as these measurements moved away from the surface and reached a distance of 170 µm below the machined surface. The greatest increase in hardness was observed after milling with grinding wheel mesh 46 (Fig. 4e) at a distance of 30 µm from the ground surface and which was 30% greater than the reference value when using the severest condition of $v_w =$

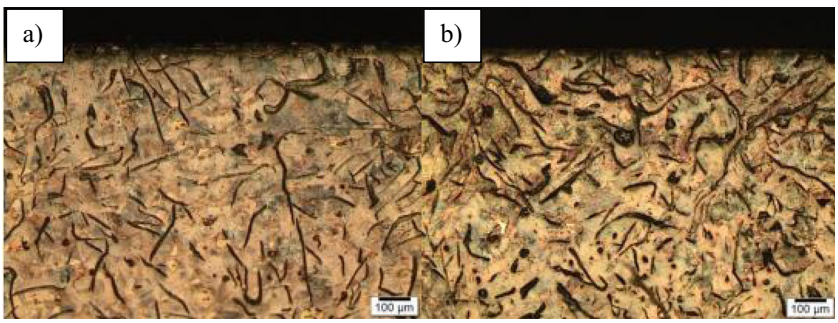

Fig. 6 Subsurface images of the GCI samples ground with grinding wheel mesh 100: **a**) 100: $a_e = 15$ µm and **b**) $a_e = 30$ µm

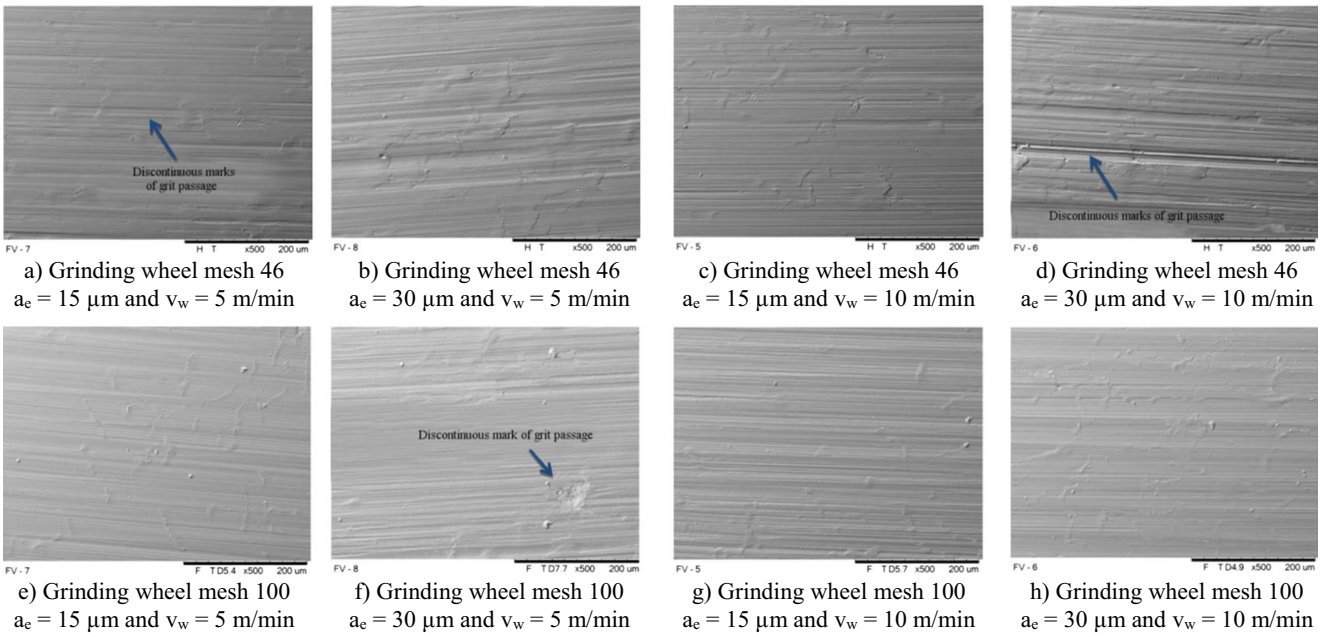

a) Grinding wheel mesh 46 a_e = 15 µm and v_w = 5 m/min
b) Grinding wheel mesh 46 a_e = 30 µm and v_w = 5 m/min
c) Grinding wheel mesh 46 a_e = 15 µm and v_w = 10 m/min
d) Grinding wheel mesh 46 a_e = 30 µm and v_w = 10 m/min
e) Grinding wheel mesh 100 a_e = 15 µm and v_w = 5 m/min
f) Grinding wheel mesh 100 a_e = 30 µm and v_w = 5 m/min
g) Grinding wheel mesh 100 a_e = 15 µm and v_w = 10 m/min
h) Grinding wheel mesh 100 a_e = 30 µm and v_w = 10 m/min

Fig. 7 Images of the surfaces for compacted graphite iron (CGI) ground under different cutting conditions. **a** Grinding wheel mesh 46; a_e = 15 µm and v_w = 5 m/min. **b** Grinding wheel mesh 46; a_e = 30 µm and v_w = 5 m/min. **c** Grinding wheel mesh 46; a_e = 15 µm and v_w = 10 m/min. **d** Grinding wheel mesh 46; a_e = 30 µm and v_w = 10 m/min. **e** Grinding wheel mesh 100; a_e = 15 µm and v_w = 5 m/min. **f** Grinding wheel mesh 100; a_e = 30 µm and v_w = 5 m/min. **g** Grinding wheel mesh 100; a_e = 15 µm and v_w = 10 m/min. **h** Grinding wheel mesh 100; a_e = 30 µm and v_w = 10 m/min

10 m/min and a_e = 15 µm. In the same region, the increase in hardness was about 24% after machining at the combination of the severest machining conditions of v_w = 10 m/min and a_e = 30 µm. For the grinding wheel mesh 100 (Fig. 4f), there was also an increase in the values of hardness initially detected in regions below 30 µm of the machined surfaces, and that also decreased for all conditions, but with a less accentuated slope in relation to mesh 46 (Fig. 4e). In addition, the percentage increase of about 20% for microhardness obtained after machining with mesh 100 was lower than that observed for mesh 46 in the region at 30 µm of the ground surface. However, with the exception of the previously mentioned condition in which mesh 46 was used, v_w = 10 m/min, a_e = 15 µm (Fig. 4e), the microhardness values for mesh 46 were closer to the reference line hardness of the material prior the grinding process when compared to those recorded after machining with the grinding wheel of larger mesh (smaller grit size). The highest values of roughness and greater percentage increase in the microhardness were obtained after the machining with the larger mesh. In relation to the increase in the microhardness values recorded for this grade of cast iron in comparison to the other grades investigated in this study, these all can be attributed to the lower thermal conductivity of nodular cast iron. This phenomenon occurs due to the different graphite present not being connected, in addition to their higher coefficient of friction, which together tend to raise the temperature during grinding. In addition, chips may become lodged in the grinding wheel during the grinding process. This causes the workpiece material present on the grinding wheel to rub against the workpiece, reducing the efficiency of the abrasive grits and increasing the generation of heat in the cutting zone. Finally, the cutting fluid may have difficulty in reaching the cutting zone to assist in the removal of heat from the principal areas of the workpiece. All these factors acting in combination lead to the generation of a higher temperature gradient on the workpiece surface. This heat causes, in turn,

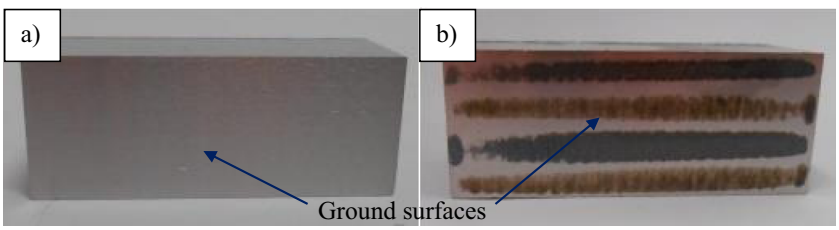

Fig. 8 Images of CGI ground surfaces with wheel: (a) 39C46KVK and (b) 39C100KVK

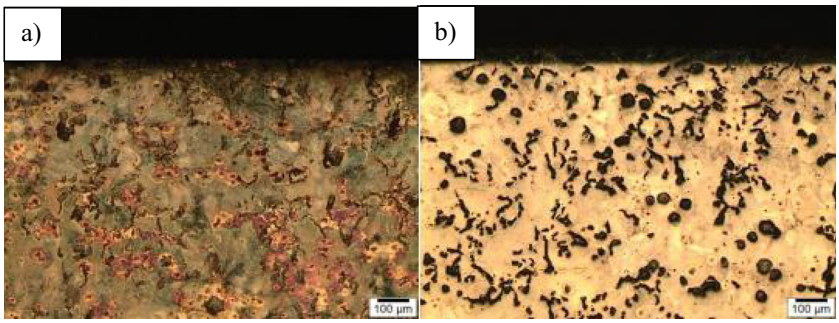

Fig. 9 Subsurface images of the samples of CGI ground with grinding wheel mesh 100: **a** $a_e = 15$ µm and **b** $a_e = 30$ µm

metallurgical alterations in regions near the ground surface. In the case of the nodular cast iron machined in this research study, it is believed that there was the formation of a non-annealed martensitic structure on the surface of the workpiece, which has a hardness value higher than the original microstructure (prior to grinding operation).

3.3 Images of the machined surfaces and microstructures

In Fig. 5a–h, the surface images of the samples showing the gray cast iron (GCI) grade machined under different cutting conditions obtained by scanning electron microscope (SEM).

The images of the gray cast iron sample surfaces after grinding under various cutting conditions are shown in Fig. 5a–h. In these images, it was noted that, regardless of the cutting conditions used, there were no changes in the texture or any surface damage and no cracks after grinding. However, there exists *n* observable plastic deformation and side flow of material from the workpiece in some regions, as a result of the passage of abrasives. Appearance of the surfaces are very similar under all the conditions tested, although the grit advance marks are more evident on the surface in which the grinding wheel mesh 46 was employed with visible scratches along the cutting direction of the tool. Under the severer conditions of machining, with higher radial depth of cut and higher worktable speed (Fig. 5d, h), one notes that the longitudinal marks on the surface are wider and with some discontinuity along the machined surface in relation to those observed after machining under milder conditions. This can be attributed to the greater effort of the grinding wheel to remove material and greater penetration of the grit on the workpiece, which adversely affects the roughness profile. Noteworthy also is the evidence of material detachment, especially in the

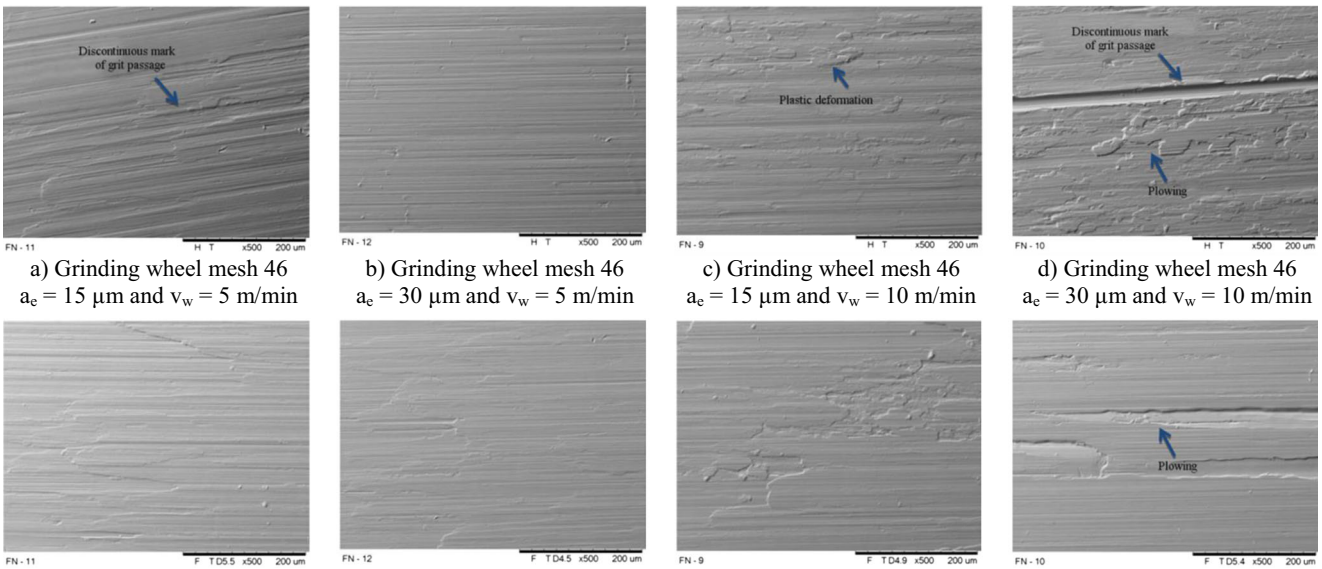

a) Grinding wheel mesh 46 a_e = 15 µm and v_w = 5 m/min
b) Grinding wheel mesh 46 a_e = 30 µm and v_w = 5 m/min
c) Grinding wheel mesh 46 a_e = 15 µm and v_w = 10 m/min
d) Grinding wheel mesh 46 a_e = 30 µm and v_w = 10 m/min
e) Grinding wheel mesh 100 a_e = 15 µm and v_w = 5 m/min
f) Grinding wheel mesh 100 a_e = 30 µm and v_w = 5 m/min
g) Grinding wheel mesh 100 a_e = 15 µm and v_w = 10 m/min
h) Grinding wheel mesh 100 a_e = 30 µm and v_w = 10 m/min

Fig. 10 Images of the surfaces of nodular cast iron (NCI) ground under different cutting conditions. **a** Grinding wheel mesh 46; $a_e = 15$ µm and $v_w = 5$ m/min. **b** Grinding wheel mesh 46; $a_e = 30$ µm and $v_w = 5$ m/min. **c** Grinding wheel mesh 46; $a_e = 15$ µm and $v_w = 10$ m/min. **d** Grinding wheel mesh 46; $a_e = 30$ µm and $v_w = 10$ m/min. **e** Grinding wheel mesh 100; $a_e = 15$ µm and $v_w = 5$ m/min. **f** Grinding wheel mesh 100; $a_e = 30$ µm and $v_w = 5$ m/min. **g** Grinding wheel mesh 100; $a_e = 15$ µm and $v_w = 10$ m/min. **h** Grinding wheel mesh 100; $a_e = 30$ µm and $v_w = 10$ m/min

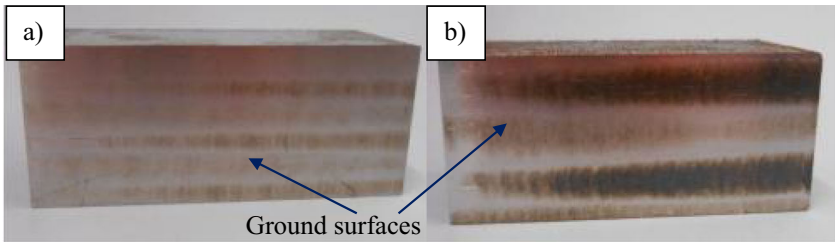

Fig. 11 Images of NCI ground surfaces with grinding wheel mesh 100 and radial depth of cut: (a) 15 and (b) 30 μm

use of grinding wheel mesh 100, which is related to the fact that it is a fragile material, with little plastic regime compared to other cast iron grades tested in this paper. With this being the case, there is a greater tendency toward detachment when a tool comes into contact with the workpiece surface. In addition, since the chips are discontinuous, there is variation in the shear forces, which negatively reflects in the finish [4].

In Fig. 6a, b, one notes the subsurface images of two samples of GCI that were generated after grinding with $a_e = 15$ μm and $a_e = 30$ μm, respectively, while $v_w = 10$ m/min and grinding wheel mesh 100 were kept constant. Noted from both images is that there is no evidence of microstructural alteration on the samples that could compromise the integrity of the material and that there was no significant difference when using two different radial depths of cut.

With respect to the compacted graphite iron, the SEM images of the different ground surfaces are shown in Fig. 7a–h. Similar to the surfaces of the gray cast iron grade (Fig. 5a–h), it was not possible to identify surface damage on the compacted graphite iron samples after grinding under the conditions tested. From Fig. 7a–d, there are notable interrupted marks on the ground surfaces, along with evidence of more material deformed than under other tested conditions, which adversely affected the roughness (Fig. 3). In addition, noted from Fig. 7d is that such a surface on which the abrasive grits produced the most pronounced grooves with deformation of material. Highlighted here is that from the first pass of the grinding wheel mesh 100 on the surface of the compacted graphite iron (CGI) grade, the presence of deep and interrupted visible marks on the surfaces was observed, thereby indicating that this grinding wheel material (SiC) is suitable for the grinding of the CGI grade under the cutting conditions used in this research paper. However, even with these marks, the grinding wheel mesh 100 resulted in a better surface finish under all conditions tested for compacted graphite iron, as well as with no significant variation of microhardness below the material surface.

In Fig. 8, two samples of CGI are shown after grinding with the same radial depth of cut and worktable speed, but with different grinding wheel meshes. From this figure, the presence of visual marks with a blue-copper coloration only on the surface after grinding with the grinding wheel mesh 100 is clearly evident (Fig. 8(b)). These results show the importance of evaluating different grinding output parameters, such as roughness, microhardness, and observation of ground surfaces, as well as being attentive during the grinding process to record any type of occurrence. The use of more than one variable helps in the analysis of results and if there is any correlation between them to explain the phenomenon involved in the grinding process.

In Fig. 9a, b, the sub-surface images are presented of two samples of CGI obtained after grinding with $a_e = 15$ μm and $a_e = 30$ μm, respectively, and under the cutting conditions $v_w = 10$ m/min and grinding wheel mesh 100. Note that there is a change in the microstructure very close to the workpiece surface. This change is more evident in Fig. 9a, using a radial depth of cut of 15 μm, which is consistent with the results obtained for the microhardness, in which the a_e generated a greater variation of microhardness near the surface, in relation to $a_e = 30$ μm. This may have occurred due to the microstructure of this material and its greater hardness (323 HV) in relation to the other cast iron types. In addition, this grade of cast iron (CGI) has a high tensile strength (524 MPa), which requires greater cutting force and consequently greater

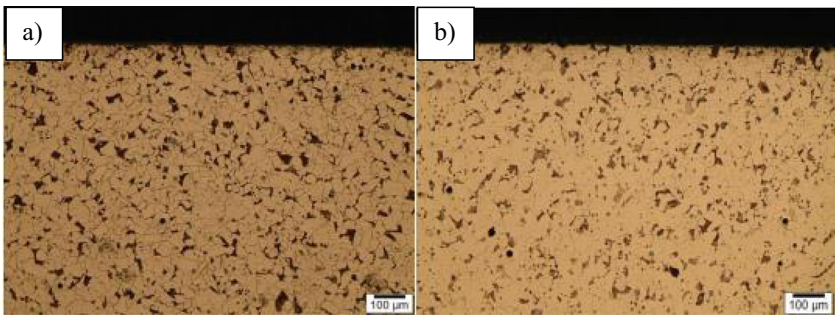

Fig. 12 Subsurface images of NCI samples ground with grinding wheel mesh 100: **a**) $a_e = 15$ μm and **b** $a_e = 30$ μm

machine power to ensure the removal of the same amount of material.

In Fig. 10a–h, the SEM surface images are shown for nodular cast iron (NCI) samples after grinding under various cutting conditions. Similar to that observed for the machined surfaces of other cast iron grades (CGI and GCI) tested in this study, the images of the surfaces via SEM, in general, did not show evidence of cracks perpendicularly to the cutting marks on the machined surface or any other damage that could compromise the integrity of the workpiece material. However, grooves can be observed on the surfaces that have been machined under severer grinding conditions (Fig. 10d, h), which are popularly known as "plowing." This mechanism is related to the characteristics of nodular cast iron (high ductility and toughness) that similarly to carbon steels with lower-medium hardness impairs the shearing and removal of the material during grinding, especially when machining under more aggressive conditions [1]. Such surface grooves adversely affect the roughness profile and appearance of the ground surface. Also, in relation to the images in Fig. 10a–h, the increase in temperature in the workpiece, as a consequence of the heat rise, probably occurred during the process with grinding wheel mesh 100, which also caused copper-colored marks in all the samples, just as that which occurred for iron (a_e) and higher workpiece velocities (v_w), which is consistent with the results found for the roughness parameter Ra, where severer machining conditions produced a worse surface finish.

Images of two samples of NCI ground with two different radial depths of cut, but with the same worktable speed (v_w = 10 m/min) and even grinding wheel (mesh 100) are shown in Fig. 11. In both, marks (burning) are observed from the grinding process, which are very evident and became severer as the radial depth of the cut increased (Fig. 11(b)).

In Fig. 12a, b, the sub-surface images of the two samples are shown for NCI, which were ground with a_e = 15 μm and a_e = 30 μm, respectively, and with v_w = 10 m/min and grinding wheel mesh 100. There was no observed formation of layers affected by heat, even though the increase of microhardness on the surface of the ground material was detected (Fig. 4) and visual burning while employing the two values of radial depth of cut as already commented previously.

4 Conclusions

After the analysis of the experimental data from this investigative study, the following conclusions can be drawn:

- The Ra parameter for the three studied cast iron grades (gray, compacted graphite, and nodular cast) increased with the radial depth of cut from 15 to 30 μm, as expected, and among the cast iron studied in this paper, the gray grade was that which demonstrated the lowest Ra roughness values across all the cutting conditions employed in this work.
- In general, all the roughness values for the Ra parameter were below 0.46 μm and the values obtained for the Ra parameter were within the acceptable roughness range for the semi-finishing grinding process, which is 0.63 μm.
- The Ra roughness parameter was more sensitive to the variation of the worktable speed than to the radial depth of cut, so that, regardless of the radial depth of cut and grit of the grinding wheel employed, the increase in speed resulted in an increase in roughness values, consequently deteriorating the surface finish. However, the combination of higher worktable speed and higher radial depth of cut generally resulted in higher roughness values, with the exception of compacted graphite iron.
- The ductility of nodular cast iron negatively reflected on the surface finish and texture of the surfaces after grinding across all the cutting conditions employed.
- The mesh of the grinding wheel influenced both the roughness values and the texture of the surfaces of the three cast iron grades. Overall, grinding with mesh 100 produced a worse surface finish for all grades of cast iron studied in this paper. In addition, grinding burns from a visual inspection aspect were observed on compacted graphite and nodular cast iron grades after machining with this mesh.
- With regard to the microhardness, in general, the values for gray cast iron remained around the average for the material value before grinding, without significant changes. However, for compacted graphite iron, there was a slight percentage drop of 1.8% in microhardness in regions closer to the ground surface, when using the highest worktable speed (v_w = 10 m/min). For nodular cast iron, the percentage increase in the microhardness values were about 30% after machining with v_w = 10 m/min and a_e = 15 μm and about 24% after using the cutting parameters of v_w = 10 m/min and a_e = 30 μm with grinding wheel mesh 46. When using grinding wheel mesh 100, the percentage increase was lower than for mesh 46. In general, with respect to nodular cast iron, the microhardness values obtained after testing grinding wheel mesh 46 were closer to the reference line, when compared to those recorded after machining with the higher grinding wheel mesh.
- Regarding the surfaces and topographies of the workpieces, there were observed regions with plastic deformation and side flow of workpiece material as a result of the passage of the abrasive grits onto the workpiece, mainly under severer conditions, with a_e = 30 μm and v_w = 10 m/min, but without the presence of cracks.
- Based on the microhardness measurements, one reaches the conclusion that there were no microstructural alterations in the samples of gray and compact graphite cast iron grades, even after machining under the severest

grinding conditions. However, for the compacted graphite iron, when a grinding wheel mesh 100 was used in combination with $v_w = 10$ m/min and $a_e = 30$ μm (severer machining conditions), a change was observed in the microstructure close to the surface.

- Based on the analyses of the results for roughness, microhardness, and surface and sub-surface images obtained in this research, the conclusion can be drawn that, in general, the use of lower values of radial depth of cut and worktable speed, in combination with the carbide silicon grinding wheel and lower mesh (larger grit size), generates reasonably good finishing and surface integrity, without damage to the cast iron grades investigated in this study.
- The microstructure and mechanical properties of the cast iron grades tested played a strong influence on their grindability in terms of the evaluated output parameters.
- The ranking order for the grindability of the three cast iron grades in terms of roughness, microhardness, and surface texture investigated in this study is gray cast iron (GCI), compacted graphite iron (CGI), and nodular cast iron (NCI).

Acknowledgements The Authors are grateful to Tupy, Saint Gobain Abrasives, and Blaser Swisslube Brazil, all Brazilian companies, for supporting this work with donation of workpiece material, grinding wheels and coolant, respectively.

Funding information The authors thank the CAPEX PROEX, FAPEMIG, and the Post Graduate Program of Mechanical Engineering of UFU for the financial support.

Compliance with ethical standards

Conflict of interest The authors declare that there is no conflict of interest.

Publisher's Note Springer Nature remains neutral with regard to jurisdictional claims in published maps and institutional affiliations.

References

1. Davis JR (1996) Cast iron. Specialty handbook
2. De Sousa JAG, Sales WF, Machado AR (2017) A review on the machining of cast irons. Int J Adv Manuf Technol 94:4073–4092. https://doi.org/10.1007/s00170-017-1140-1
3. Callister WD, Rethwisch DG (2013) Materials science and engineering, 9th edn. Wiley, New York
4. Marinescu ID, Hitchiner M, Uhlmann E, Rowe WB, Inasaki I (2007) Handbook of machining with grinding wheels. CRC Press, Nova Iorque
5. Mocellin F, Melleras E, Boehs L, Guesser WL (2004) Study of the machinability of compacted graphite iron for drilling process. J Braz Soc Mech Sci Eng 26:22–27. https://doi.org/10.1590/S1678-58782004000100004
6. Malkin S, Guo C (2008) Grinding technology: theory and applications of machining with abrasives, 2nd edn. Industrial Press, New York
7. Klocke F (2009) Manufacturing process 2: grinding, honing, lapping. Ed Springer
8. Moltrecht KH (1981) Machine shop practice, 2nd edn. Industrial Press, New York
9. Sosa AD, Echeverría MD, Moncada OJ, Sikora JA (2007) Residual stresses, distortion and surface roughness produced by grinding thin wall ductile iron plates. Int J Mach Tools Manuf 47:229–235. https://doi.org/10.1016/j.ijmachtools.2006.04.004
10. Xiao G, Stevenson R, Hanna IM, Hucker AS (2002) Modeling of residual stresses in grinding of nodular cast iron. ASME J Manuf Sci Eng 124:833
11. Fernandes LM, Lopes JC, Volpato RS, Diniz AE, De Oliveira RFM, De Aguiar PR, De Mello HJ, Bianchi EC (2018) Comparative analysis of two CBN grinding wheels performance in nodular cast iron plunge grinding. Int J Adv Manuf Technol. https://doi.org/10.1007/s00170-018-2133-4
12. Elliot R (1988) Cast iron technology. Butterworth & Co. Ltd
13. TUPY (2018) Continuous cast iron bars. Available at http://www.tupy.com.br/ingles/produtos/perfis_processo.php
14. Brooks R (2012) SinterCast logs new order for Tupy in Mexico. Foundry Management & Technology, United States of America. Available at: https://www.foundrymag.com/meltpour/sintercast-logs-new-order-tupy-mexico
15. Dawson S, Schroeder T (2004) Practical applications for compacted graphite iron. AFS Transactions, 04–047(05):1–9. Des Plaines, IL USA
16. Rowe WB (2014) Principles of modern grinding technology. 2nd ed. Elsevier Inc.
17. Marinescu ID, Rowe WB, Dimitrov B, Inasaki I (2004) Tribology of abrasive machining processes, 1st edn. William Andrew Inc, Norwich
18. Dawson S, Hollinger I, Robbins M, Daeth J, Reuter U, Schulz H (2001) The effect of metallurgical variables on the machinability of compacted graphite iron. Society of Automotive Engineers
19. Astakhov VP, Joksch S (2012) Metalworking fluids (MFWs) for cutting and grinding—fundamentals and recent advances. Woodhead, Cambridge
20. Pereira AA, Boehs L, Guesser WL (2006) The influence of sulfur on the machinability of grey cast iron FC25. J Mater Process Technol 179:165–171. https://doi.org/10.1016/j.jmatprotec.2006.03.100
21. Marwanga RO, Vogt RC, Cohen PH (2000) Influence of graphite morphology and matrix structure on chip formation during machining of continuously cast ductile irons. AFS Transactions, Des plaines
22. Fathallah BB, Fredj NB, Sidhom H, Braham C, Ichida Y (2009) Effects of abrasive type cooling mode and peripheral grinding wheel speed on the AISI D2 steel ground surface integrity. Int J Mach Tools Manuf 49:261–272. https://doi.org/10.1016/j.ijmachtools.2008.10.005